Journal of Industrial and Engineering Chemistry 46 (2017) 304–314

Contents lists available at ScienceDirect

Journal of Industrial and Engineering Chemistry

journal homepage: www.elsevier.com/locate/jiec

Effect of conjugated 2D-side groups on quinacridone-based copolymers to adjust deep HOMO level for photovoltaics

Hyun Ah Sung, Doo Hun Kim, Tae Ho Lee, Min Hee Choi, Eui Jin Lee, Doo Kyung Moon*

Department of Materials Chemistry and Engineering, Konkuk University, 1 Hwayang-dong, Gwangjin-gu, Seoul 143-701, Republic of Korea

ARTICLE INFO

Article history:
Received 26 August 2016
Received in revised form 12 October 2016
Accepted 29 October 2016
Available online 8 November 2016

Keywords:
Bulk heterojunction polymer solar cells
Conjugated 2D-side groups
Suzuki coupling reaction
Deep HOMO level

ABSTRACT

Different conjugated 2D-side groups were introduced to polymerize four types of two-dimensional polymers, PQCT-m8Qx, PQCT-mEHQx, PQCT-BT and PQCT-DPP, through a Suzuki coupling reaction. In comparison with the linear polymer which used the same backbone, the two-dimensional (2D) conjugated side chain polymer exhibits the delocalization of its electron clouds due to the extension of the side chain. So, all four polymers showed a low HOMO level, thus showing high V_{OC}. Among the four, the HOMO level of PQCT-BT was the lowest, by −5.63 eV. When manufacturing a device, V_{OC} was 0.92 V, which is the highest.

Introduction

Polymer solar cells (PSCs) are capable of solution processes and can be manufactured at low price. Additionally, they are lightweight, flexible, and are advantageous in large-area-scaling. For these reasons, PSCs have been drawing much attention in the academic and industrial sectors. Among the PSCs, the bulk heterojunction (BHJ) system, wherein electron-donors (conducting polymers) and electron-acceptors (fullerene derivatives) are blended, have contributed much to the enhancement of photovoltaic performance and have been studied in various ways [1,2]. In the BHJ system, through rational design of the conjugated backbone or side chains, PSCs with high efficiency can be realized. To obtain high power conversion efficiency (PCE), the open circuit voltage (V_{OC}), short circuit current (J_{SC}) and fill factor (FF) should be increased [3]. In particular, since a conjugated polymer of the donor–acceptor (D–A) type is capable of tuning the energy level in accordance with the acceptor's chemical structure, it has been used in various PSCs [4,5]. For a time, many studies focused on how to reduce the band gap of the D–A type polymer because J_{SC} can be increased by the improvement of photon harvesting property. However, since such structures cause a decrease in V_{OC} due to a high highest occupied molecular orbital (HOMO) energy level, the PCE can be limited, due to an imbalance between V_{OC} and J_{SC} [6]. To complement this, recent studies focus on wide-bandgap (WBG, $E_g > 1.8$ eV) polymers, and reports detail the existence of polymers with the efficiencies over 5–9% [7–9].

Since V_{OC} is determined by the difference between the HOMO energy level of the donor and the LUMO energy level of the acceptor, decreasing the HOMO energy of the donor polymer becomes the major factor for enhancing the V_{OC} [10,11]. For a structure with a low HOMO energy level (deep HOMO level < -5.2 eV), a polymer design which utilizes a weak donor and a strong acceptor, has been mainly used so far [12,13]. Recently, many research groups are conducting studies focused on decreasing the HOMO energy level by using a newly structured conjugated side groups or bulky side chain [14,15]. The two-dimensional (2D) conjugated side-chain polymer, in comparison with the linear polymer, possesses the following characteristics: (1) the extension of π-conjugation; (2) good solubility due to the overlap caused by the interaction between the conjugated side chains and the main chains; and (3) a low HOMO energy level for a high open-circuit voltage (V_{OC}) [16–18]. Peng et al. introduced benzothiadiazole as a conjugated 2D-side group, and obtained a highly efficient HOMO energy level of 5.45 eV and V_{OC} of 1.0 V [19–21].

Quinacridone derivatives are well-known red–violet pigments, with ordered structure and self-assembled characteristics that are capable of serving as electron donors. Due to their high hole mobility, they have drawn great attention in OTFTs [22]. The

* Corresponding author. Fax: +82 2 444 0765.
E-mail address: dkmoon@konkuk.ac.kr (D.K. Moon).

http://dx.doi.org/10.1016/j.jiec.2016.10.044
1226-086X/

Takimiya group reported a paper wherein a polymer composed of quinacridone derivatives in possession of high hole mobility ($0.2\ cm^2\ V^{-1}\ S^{-1}$) is applied to OTFTs [23]. Quinoxaline derivatives are widely used as electron-accepting units because of their superior electron-withdrawing properties, which are caused by two imine nitrogen atoms. In addition, the quinoxaline derivatives generally have high solubility and are easily transformed structurally. Their electronic properties can also be modified by adding various substituents [24]. Since benzothiadiazole derivatives, due to their coplanar symmetrical structure, have strong electron affinity, they can be highly utilized as an acceptor. Benzothiadiazole derivatives have very strong electron affinity as the electron acceptor. And with thiophenes, rich in electrons, they connected to each terminal to increase the effective π-conjugation length. Thereby it is rational design of a basic molecular structure that produces a polymer with a low bandgap [25]. Recently, diketopyrrolopyrrole derivatives have become popular as the building blocks of polymers, oligomers, and small molecules designed to obtain high-mobility photovoltaic devices. Additionally, diketopyrrolopyrrole derivatives have well conjugated structures with strong π–π interactions and electron-withdrawing effects, which results in efficient charge transport [19,26].

In this study, the quinacridone is used as a donor, and four types of acceptors are introduced as conjugated 2D-side groups to polymerize the four types of polymers: poly[quinacridone-alt-dithienylvinyl-2,3-bis(3-octyloxy)quinoxaline] (PQCT-m8Qx); poly[quinacridone-alt-dithienylvinyl-2,3-bis(3-ethylhexyloxy) quinoxaline] (PQCT-mEHQx); poly[quinacridone-alt-dithienylvinyl-5,5-bis(octyloxyl)benzothiadiazole] (PQCT-BT); and poly [quinacridone-alt-dithienylvinyl-2,5-bis(2-ethylhexyl)diketopyrrolopyrrole] (PQCT-DPP). The thermal stabilities, optical properties, electrochemical properties and film morphologies of the polymers, by the 2D-side group, were analyzed. When PQCT-BT was introduced as an active layer, PCE = 2.2%, in PQCT-BT:$PC_{70}BM$ (1:2, w/w %).

Results and discussion

Synthesis and characterization of polymers

The monomers, polymers and their general polymerization processes are shown in Scheme 1. To enhance the solubility of the resulting polymers, side chains were introduced to the acceptors, which are 2D-side groups. As shown in Scheme 1, M2 and M3 were introduced with a linear alkoxy side chain, and a branched alkoxy side chain, respectively, at the meta position of the phenyl ring. Finally, thiophene was used as a conjugated linker to the acceptor introduced with side chain, to synthesize 5-(5-(2-(2,5-dibromothiophen-3-yl)vinyl)thiophen-2-yl)-2,3-bis(3-(octyloxy)phenyl)-8-(thiophen-2-yl)quinoxaline (M2), 5-(5-(2-(2,5-dibromothiophen-3-yl)vinyl)thiophen-2-yl)-2,3-bis(3-(2-ethylhexyloxy)phenyl)-8-(thiophen-2-yl)quinoxaline (M3), 4-(5-(2-(2,5-dibromothiophen-3-yl)vinyl)thiophen-2-yl)-5,6-bis(octyloxy)-7-(thiophen-2-yl)benzothiadiazole (M4), and (5-(2-(2,5-dibromothiophen-3-yl)vinyl)thiophen-2-yl)-2,5-bis(2-ethylhexyl)-6-(thiophen-2-yl)pyrrolopyrrole-1,4-dione (M5) in accordance with the literature [20,27–29].

As shown in Scheme 1, poly[quinacridone-alt-dithienylvinyl-quinoxaline] (PQCT-m8Qx, PQCT-mEHQx), poly[quinacridone-alt-dithienylvinyl-benzothiadiazole] (PQCT-BT), and poly[quinacridone-alt-dithienylvinyl-diketopyrrolopyrrole] (PQCT-DPP) were synthesized through a Suzuki coupling reaction, using M1 and M2 through M5. The polymerization of the four polymers was performed for 24 h at 90–95 °C using toluene as the solvent, Pd $(PPh_3)_4$ as the catalyst, 2 M aqueous potassium carbonate solution as the base and Aliquat 336 as the surfactant. After the polymerization, the polymers were end-capped with 2-bromothiophene. The polymers were precipitated into methanol for recovery. The purification was conducted in the order of methanol, acetone, and chloroform using Soxhlet extraction. Finally, the chloroform fraction was precipitated into methanol for the recovery of the polymer. As a result, the yields of PQCT-m8Qx, PQCT-mEHQx, PQCT-BT, and PQCT-DPP were, respectively, 85%, 86%, 81% and 83%. The structure of the synthesized polymers was confirmed via elemental analysis (EA). The synthesized polymer structures were further analyzed by ^1H NMR and and shown in Fig. S1. Except for PQCT-DPP, the polymers were readily soluble in general organic solvents such as tetrahydrofuran (THF), chloroform ($CHCl_3$), chlorobenzene (CB) and *o*-dichlorobenzene (*o*-DCB). PQCT-DPP was completely dissolved at elevated temperature.

The molecular weights of the obtained polymers are collected in Table 1. As shown in Table 1, the number average molecular weights (Mn) of PQCT-m8Qx, PQCT-mEHQx, PQCT-BT and PQCT-DPP were 21.4, 14.1, 47.2 and 22.6 kDa, respectively, while the polydispersity indices (PDI) were 2.85, 3.11, 2.24 and 3.04. Although PQCT-m8Qx and PQCT-mEHQx exhibited increased solubility upon introduction of the alkoxy side chain, their molecular weights were measurably lower due to steric hindrance. The steric hindrance directly impacts the polymer molecular weight, a dominant factor in determining the chain packing and mechanical properties of polymer thin films [30,31]. In comparison with the other three polymers, PQCT-BT shows high polymerization degrees. This is because the solubility was increased by introducing an alkoxy side chain to benzothiadiazole (M4), which was used as the 2D-side group [32]. In case of PQCT-DPP, the low solubility resulted in a low molecular weight. By using TGA, the thermal stability of the polymer was evaluated, and shown in Fig. S2. As a consequence of the TGA measurement of all the polymers, the temperatures inducing 5% weight thermal loss under N_2 atmosphere ranged from 322 °C to 380 °C. All the synthesized polymers possessed excellent thermal stability, confirming that they are appropriate for both the device fabrication and application in optoelectronics.

Optical properties

To examine effects of the 2D-side group on the optical properties of quinacridone-based polymers, the normalized UV–vis absorption spectra of the four polymers in diluted chloroform solution and as a thin film are shown in Fig. 1, and the results are arranged in Table 2. As indicated in Fig. 1, PQCT-m8Qx, PQCT-mEHQx, PQCT-BT and PQCT-DPP showed absorption peaks between 300–700 nm. Except for PQCT-DPP, the polymers exhibit peaks stemming from the π–π* transition of the donor segments, and shoulder peaks stemming from intramolecular charge transfer (ICT) between the conjugated backbones and their respective pendant acceptor groups [33]. In the PQCT-m8Qx and PQCT-mEHQx solutions, the maximum absorption peaks and shoulder peaks were observed at 398, 520 nm, and at 393, 510 nm, respectively. The maximum absorption peaks and shoulder peaks of the two polymer films were, respectively, 403, 547 nm, and 394, 518 nm, which are similar to the solution spectra. PQCT-m8Qx has

Table 1
Physical and thermal properties of polymers.

Polymer	Yield [%]	Mn[a] [kDa]	Mw[a] [kDa]	PDI[a]	T_d[b] [°C]
PQCT-m8Qx	85	21.4	61.4	2.85	380
PQCT-mEHQx	88	14.1	44.0	3.11	356
PQCT-BT	82	47.2	103.0	2.24	322
PQCT-DPP	83	22.6	68.9	3.04	348

[a] Determined by GPC in chloroform ($CHCl_3$) using polystyrene standards.
[b] Temperature resulting in 5% weight loss based on the initial weight.

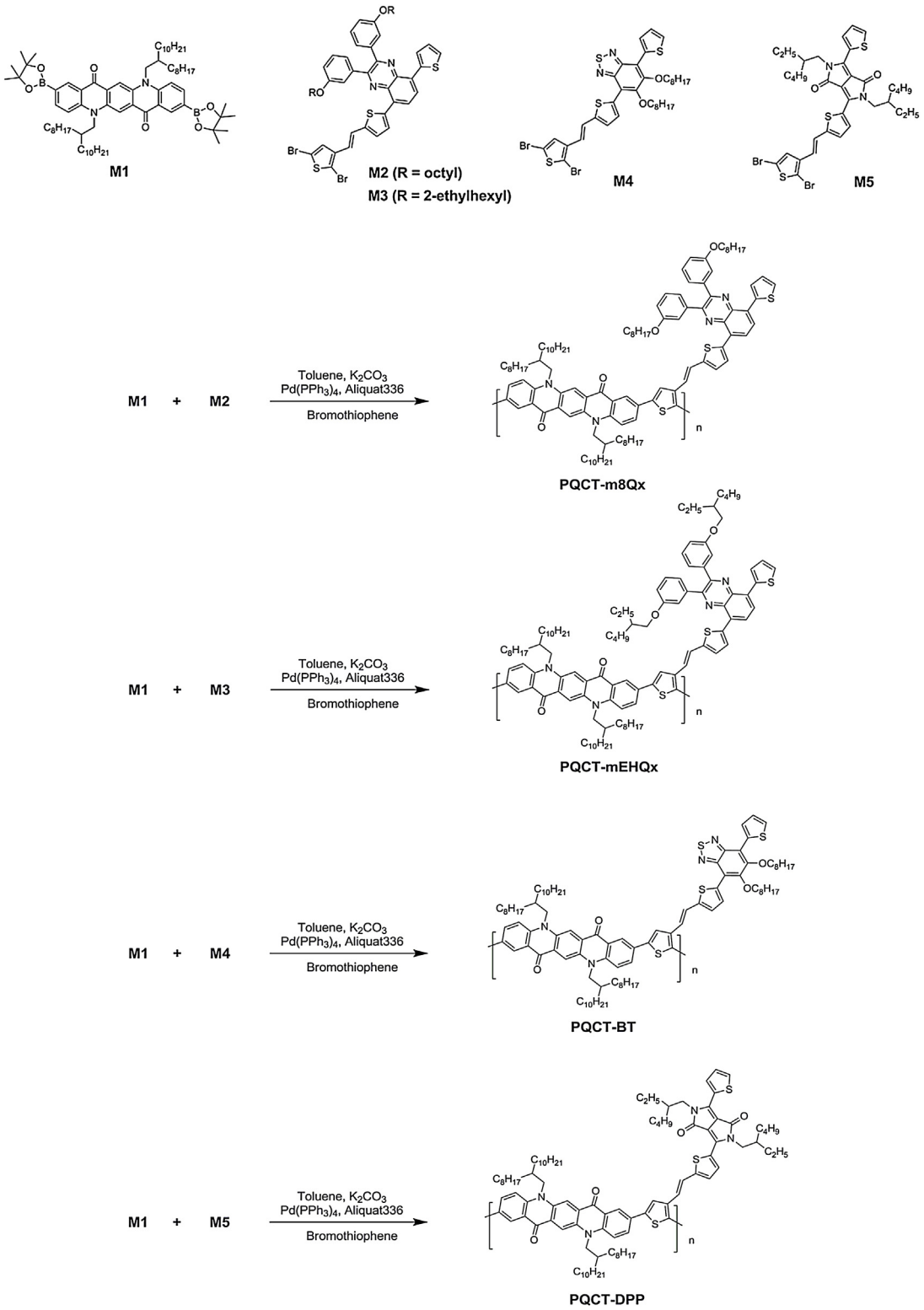

Scheme 1. Scheme of polymerization.

higher molecular weight than does PQCT-mEHQx, and exhibits enhanced aggregation, and the absorption spectrum reflects a stronger intensity and a red-shift of approximately 29 nm [34]. In the solution spectra of PQCT-BT and PQCT-DPP, the maximum absorption peaks were observed at 417, 506 nm, and at 410, 563 nm, respectively. In the films, the maximum absorption peaks were located at 410, 548 nm, and at 408, 566, 629 nm. After comparison with the solution spectra, red-shifts of approximately 42, and 66 nm were confirmed. In the cases of PQCT-BT and PQCT-DPP, the aggregation and π–π intermolecular interactions in polymer main chain in the solid state were stronger than in the polymers introduced with quinoxaline. Through this, it can be estimated that PQCT-BT and PQCT-DPP, in comparison with PQCT-m8Qx and PQCT-mEHQx, showed lower steric hindrance, excellent

Table 2
Optical and electrochemical properties of polymers.

Polymer	UV–vis absorption			Cyclic voltammetry		
	$CHCl_3$ solution [nm] λ_{max} [nm]	Film [nm] λ_{max} [nm]	$E_g^{opt,a}$ [eV]	E_{ox}^{onset} [V]	HOMO[b] [eV]	LUMO[b] [eV]
PQCT-m8Qx	398, 520	403, 547	2.05	1.24	−5.50	−3.45
PQCT-mEHQx	393, 510	394, 518	2.05	1.18	−5.43	−3.38
PQCT-BT	417, 506	410, 548	2.06	1.37	−5.62	−3.56
PQCT-DPP	410, 563	408, 566, 629	1.82	1.12	−5.37	−3.55

[a] Calculated from the intersection of the tangent on the low energetic edge of the absorption spectrum with the baseline.
[b] $E_{HOMO\ (or\ LUMO)} = -[E_{onset}(vs\ Ag/AgCl) - E_{1/2}(Fc/Fc+vs\ Ag/AgCl)] - 4.8$ eV.

planarity and expanded π–π stacking of the polymers [35]. PQCT-DPP, unlike the other three polymers, showed a clear peak, which is caused by the intramolecular charge transfer (ICT) transition between the donor–acceptor at a relatively lower energy region (563 nm). It is because the diketopyrrolopyrrole monomer is a brilliant red dye, and possesses strong electron withdrawing properties [29,30].

Fig. S3 contains the UV–vis absorption spectra of PQCT-m8Qx, PQCT-mEHQx, PQCT-BT and PQCT-DPP in diluted $CHCl_3$ solutions at various concentrations and a calculation of the molar absorption coefficients (ε). The absorption coefficients calculated at the maximum absorption peak (λ_{max}) of each polymer in solution were $7.0 \times 10^4\ M^{-1}\ cm^{-1}$ for PQCT-m8Qx, $6.4 \times 10^4\ M^{-1}\ cm^{-1}$ for PQCT-mEHQx, $9.9 \times 10^4\ M^{-1}\ cm^{-1}$ for PQCT-BT and $5.6 \times 10^4\ M^{-1}\ cm^{-1}$ for PQCT-DPP. The polymers' E_g^{opt} calculated from λ_{onset} of the solid state films of PQCT-m8Qx, PQCT-mEHQx and PQCT-BT were 2.05, 2.05, and 2.06 eV, respectively, which are similar. PQCT-DPP, due to its strong electron withdrawing and wide absorption range, showed relatively lower band gap of 1.82 eV.

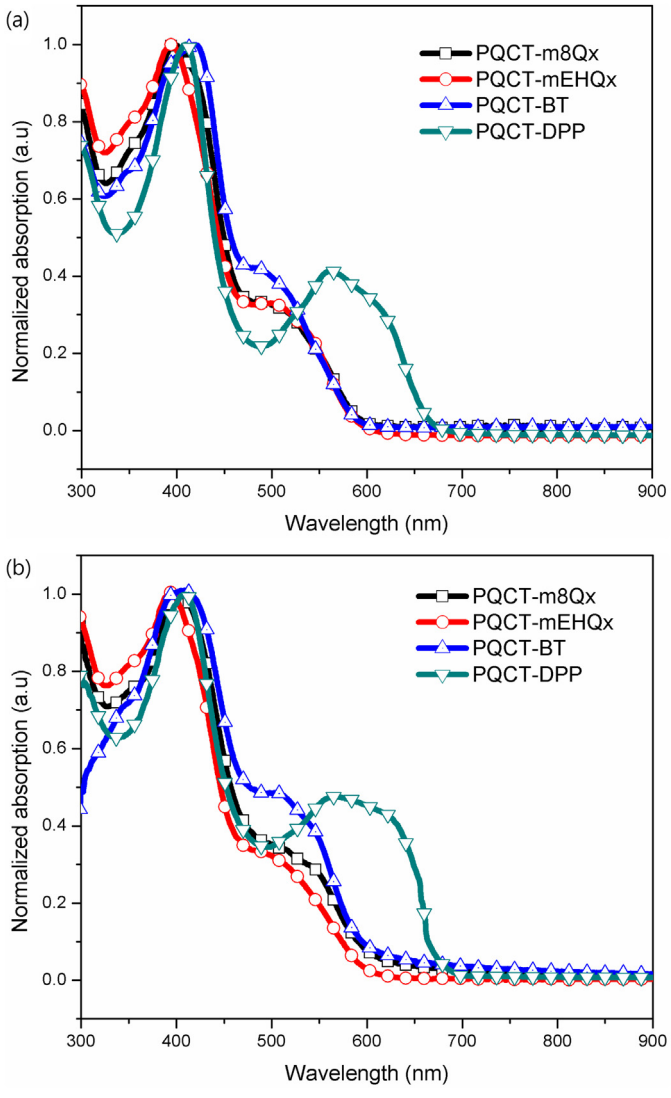

Fig. 1. Normalized UV–vis absorption spectra of polymers in (a) solution and (b) film.

Electrochemical properties

Cyclic voltammograms (CVs) were used to determine the electronic energy levels of the polymer films. Measurements were taken in a 0.1 M tetrabutylammonium-hexafluorophosphate/acetonitrile solution, and the results are shown in Fig. 2 and Table 2. The HOMO energy levels of PQCT-m8Qx, PQCT-mEHQx, PQCT-BT and PQCT-DPP were calculated as −5.50 eV, −5.43 eV, −5.63 eV and −5.37 eV, with ferrocene as the internal standard, using the equation $\{E_{HOMO}\ (eV) = -4.8 - (E_{onset} - E_{1/2}(Ferrocene)\}$. All four polymers showed HOMO energy levels lower than the air oxidation threshold (−5.20 eV). Therefore, PQCT-m8Qx, PQCT-mEHQx, PQCT-BT and PQCT-DPP are expected to possess good oxidative stability [36,37]. In the cases of PQCT-m8Qx and PQCT-mEHQx, although they incorporate the same donor, due to the difference in the side-chain structure of quinoxaline, the acceptor unit, their HOMO energy levels were different. This is due to the low molecular weight caused by the steric hindrance in PQCT-mEHQx, which led to higher HOMO energy level [38]. PQCT-DPP, in comparison with the other three polymers, showed a higher HOMO energy level. This is due to the relatively high molecular energy level of the DPP unit (HOMO, and the LUMO energy levels of DPP are −5.3 eV, and −3.4 eV) [39]. V_{OC} of BHJ PSCs is determined by the difference

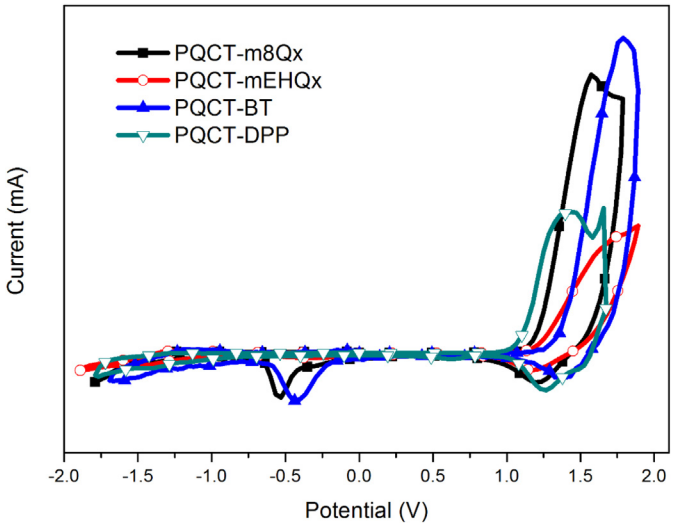

Fig. 2. Cyclic voltamograms of polymers.

between the HOMO level of the p-type, and the LUMO level of the n-type. Therefore, the device introduced with PQCT-m8Qx and PQCT-BT as the donor, which showed deep-lying HOMO energy levels, is expected to have high V_{OC} values. The LUMO energy levels were calculated as the difference in the optical band gap (E_g^{opt}) between the HOMO energy level, and these were determined to be −3.45 eV, −3.38 eV, −3.56 eV and 3.55 eV, respectively. The LUMO gaps of 0.34–0.52 eV between the copolymers and $PC_{70}BM$ would afford a sufficient driving force to facilitate an efficient exciton dissociation at the D–A interface, thereby ensuring energetically favorable electron transfer able to overcome the binding energy of the intrachain exciton [21].

Theoretical calculations

To understand the electric properties of the polymers, density functional theory (DFT) methods were used to simulate the distribution of the electron density of states (Fig. 3), molecular geometries and dihedral angles (Table 3). DFT was used for the simulation. The DFT calculation used hybrid B3LYP correlation functional, and the split valence 6-31G(d) basis set as implemented in the Gaussian 09 suite of programs. For simplification of the computations, the polymer backbones were reduced to oligomers with a single repeating unit. In Fig. 3, the HOMOs of all four types of polymers are localized in the thiophene unit including the 2D-side group, rather than delocalized over the entire polymer main backbone. This indicates that the thiophene unit works more as a donor than the quinacridone unit. The LUMOs have more electron clouds localized by acceptor cores other than the thiophene link. This is due to the structural characteristics of forming quinoid structures, the unshared electron pair of nitrogen, and the electron withdrawing capacity of sulfur [40]. PQCT-m8Qx and PQCT-mEHQx, unlike PQCT-BT and PQCT-DPP, had electron clouds in the quinacridone core in the LUMOs. This means that the quinacridone does not possess donor characteristics, but is rather electron-withdrawing. This is because, according to the report of Chen et al., the quinacridone core can act as a donor or an acceptor under different conditions, depending on the electron affinity of the attached units [41,42]. Additionally, since quinoxaline as an acceptor, in comparison with DPP and BT, has a weaker electron-withdrawing capability, the electron clouds in the electron density shapes of the LUMO orbitals could even be expanded onto the quinacridone core. Through the electron cloud distributions of the HOMOs and LUMOs, the external excitations from the thiophene in the 2D-side group toward the acceptor core were confirmed.

Table 3
Calculated dihedral angles of polymers.

Polymers	Dihedral angle 1 (deg)	Dihedral angle 2 (deg)
PQCT-m8Qx	−23.8	40.0
PQCT-mEHQx	−23.8	−44.0
PQCT-BT	−24.2	0.34
PQCT-DPP	−28.8	0.31

The calculated HOMO/LUMO energy levels of PQCT-m8Qx, PQCT-mEHQx, PQCT-BT and PQCT-DPP were, respectively –4.80 eV/−2.10 eV, −4.80 eV/−2.15 eV, −4.85 eV/−2.50 eV and −4.85 eV/−2.48 eV. Generally, the donor unit determines the HOMO energy level of a D–A type copolymer. In contrast to the fact that PQCT-mEHQx, due to its low molecular weight, showed a high HOMO energy level as determined by CV, the DFT calculation results suggest that all four polymers showed a similar HOMO level, due to the use of identical donor type.

Table 3 contains the dihedral angles of the four polymers, while Fig. 4 shows the side view of the backbone. Within the two repeating units, the dihedral angles (θ_1/θ_2) between the donor and

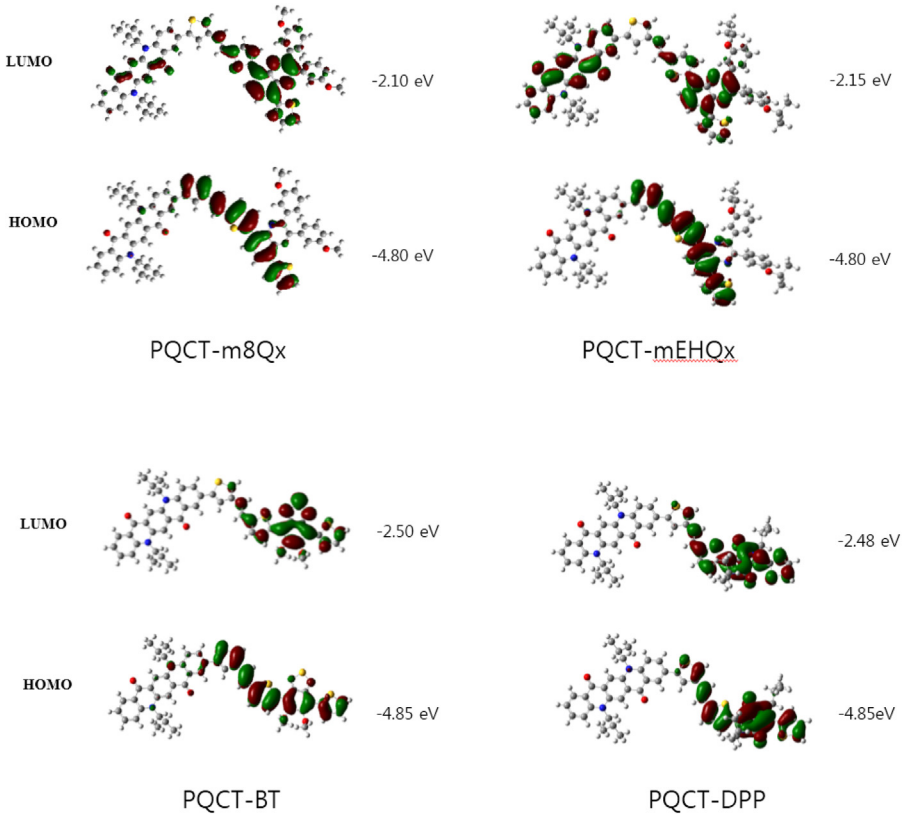

Fig. 3. Calculated HOMO and LUMO orbitals of polymers.

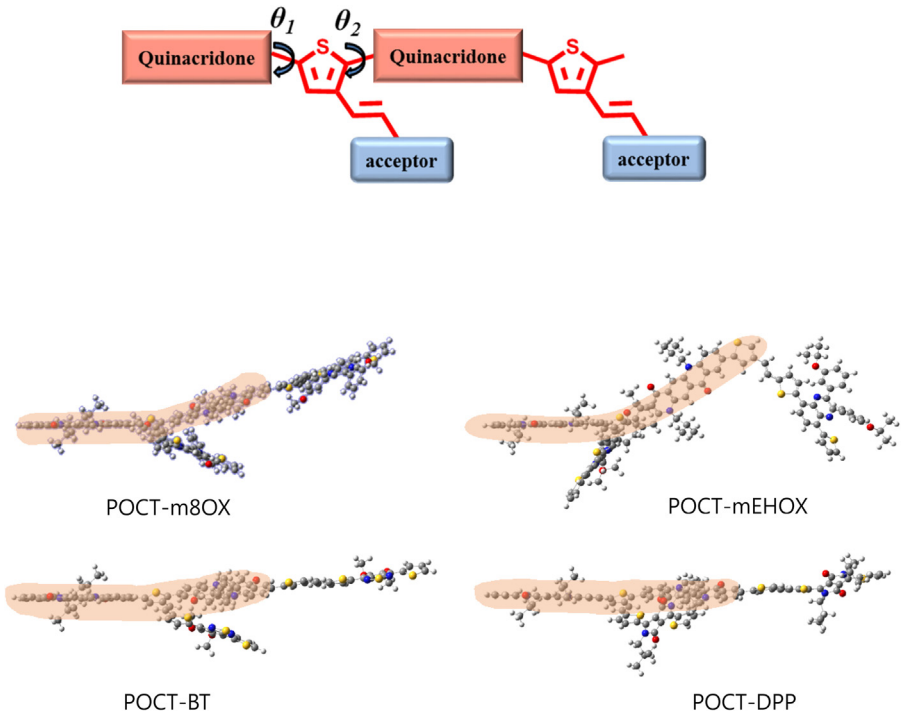

Fig. 4. Side view of the optimized geometries of the backbone of polymers.

spacer of each polymer were −23.8°/40.0°, −23.8N°/−44.0°, −24.2°/0.34° and −28.8°/0.31°. θ_1, which is directionally opposite to that of the 2D-side group, was similar in all four polymers. On the other hand, θ_2 of PQCT-BT and PQCT-DPP were smaller than those of PQCT-m8QX and PQCT-mEHQx, depending on the types of the 2D-side group. The side views revealed that PQCT-m8Qx and PQCT-mEHQx showed a curved structure, due to the steric hindrance between the repeating units. PQCT-BT and PQCT-DPP, as shown in the side view, had linear structures, and this implies that they have high planarity. Although PQCT-mEHQx introduced the monomers (quinacridone and quinoxaline) of the chemical structure, which are similar to those of PQCT-m8Qx, larger dihedral angles were shown, due to the branch alkoxy side chain.

XRD measurement

To understand the chemical structure of the polymers and the ordering and crystallinity of thin films, X-ray measurements were performed at annealing temperatures. Fig. 5(a) shows the X-ray diffraction patterns of pristine films measured in out-of-plane mode for an analysis of polymer ordering and structure.

In the out-of-plane mode, PQCT-mEHQx and PQCT-DPP showed their small diffraction peaks, respectively at 3.84°and 4.62°, in (100) plane. Through the calculations using the Bragg's law ($\lambda = 2d\sin\theta$), (100) the lamellar d-spacings (d_1) were, respectively 23.01 Å and 19.13 Å. This indicates that the two polymers form a (h00) lamellar structure, while no (0h0) peak was found. However, PQCT-m8Qx and PQCT-BT exhibited two diffraction peaks, a broad diffraction peak on the (100) and (010) crystal planes. This indicates that the polymers form (h00) lamellar structure and (0h0) lamellar structure. At the position of (100), PQCT-m8Qx and PQCT-BT show their peaks at 3.0° and 3.94°, respectively, while the ordered (100) lamellar d-spacing (d_1) were 29.45 Å and 22.43 Å, respectively. Furthermore, on the (010) plane, the π–π stacking peaks of PQCT-m8QX and PQCT-BT were observed at 20.90° and 21.18°. Therefore the π–π stacking distances (d_π) were 4.25 Å and 4.19 Å, respectively. As a result, PQCT-BT and PQCT-DPP showed smaller d_1 and d_π spacings than PQCT-m8Qx and PQCT-mEHQx, indicating stronger intra-/inter-molecular interactions. This is in agreement with the theoretical calculations in which PQCT-BT and PQCT-DPP, with low dihedral angles, form linear structures. Additionally, based on the intensity of the XRD diffraction peaks, it can be confirmed that PQCT-m8Qx, and PQCT-BT form a mixed orientation film wherein the edge and face-on structures are mixed. Since the peaks were observed on the (010) plane of the out-of-plane mode, the crystal structure inside the polymer thin film might adopt the face-on orientation. To confirm this, the X-ray diffraction of the in-plane mode was measured.

Fig. 5(b) shows the X-ray diffraction of PQCT-m8Qx and PQCT-BT thin films measured by the in-plane mode. As a result, both polymers showed crystal peaks at high and low angles of 20–25° and 3.5°, which indicates that the edge-on and face-on crystallites co-exist inside the polymer thin films (crystallite with bimodal form). PQCT-m8QX displayed a peak at higher angles rather than in lower angles, indicating that the edge-on structure is dominant. On the other hand, in the case of PQCT-BT, the crystal peak at low angles showed higher intensity rather than at high angles. This means that, within the bimodal structure, the face-on structure is more dominant [43].

Photovoltaic properties and morphology analysis

The photovoltaic properties of the polymers were evaluated by manufacturing PSC devices with an ITO/ZnO/polymer:$PC_{70}BM$/MoO_3/Ag inverted structure. All the manufactured devices were encapsulated inside a glove box. Their current density vs. voltage (J–V) characteristics were measured under ambient atmosphere with an active area of 7 mm^2. The weight ratio of polymer:$PC_{70}BM$ was altered during the measurement and 1,2-dichlorobenzene (*o*-DCB) was used as a solvent. Under all the conditions, four individual devices were tested. At the optimized weight ratio (1:2) of the polymers, J–V curves are shown in Fig. 6(a) and IPCE at the time is shown in Fig. 6(b). The photovoltaic properties of the manufactured PSCs are arranged in Table 4.

Table 4
Photovoltaic properties of polymers.

Polymer	$PC_{70}BM$ ratios	V_{oc} [V]	J_{sc} [mA/cm^2]	FF [%]	PCE [%]
PQCT-m8Qx	1:2	0.88	3.4	49.0	1.5
PQCT-mEHQx	1:2	0.80	2.7	36.5	0.9
PQCT-BT	1:2	0.92	5.3	44.8	2.2
PQCT-DPP	1:2	0.76	2.0	33.7	0.6

As shown in Table 4, in case of PQCT-m8Qx, the open circuit voltage (Voc) was 0.88 V, short-circuit current density (Jsc) was 3.4 mAcm^2, FF was 49.0% and PCE = 1.5%. PQCT-mEHQx showed Voc as 0.80 V, Jsc as 2.7 mA/cm^2, FF as 36.5% and PCE = 0.9%, while PQCT-BT showed Voc as 0.92 V, Jsc as 5.3 mA/cm^2, FF as 44.8%, thus PCE = 2.2%. However, PQCT-DPP showed V_{OC} as 0.76 V. Due to limited solubility, J_{SC} and FF were reduced, respectively, to 2.0 mA/cm^2 and 33.7%, thus resulting in PCE as 0.6% [44]. V_{OC} was calculated as the difference between the HOMO energy level of the polymer and the LUMO energy level of PCBM. The V_{OC} of the fabricated devices showed a tendency similar to that of the HOMO level measured from CV. PQCT-m8Qx and PQCT-BT showed a low HOMO energy level below −5.5 eV, which led to high V_{OC}.

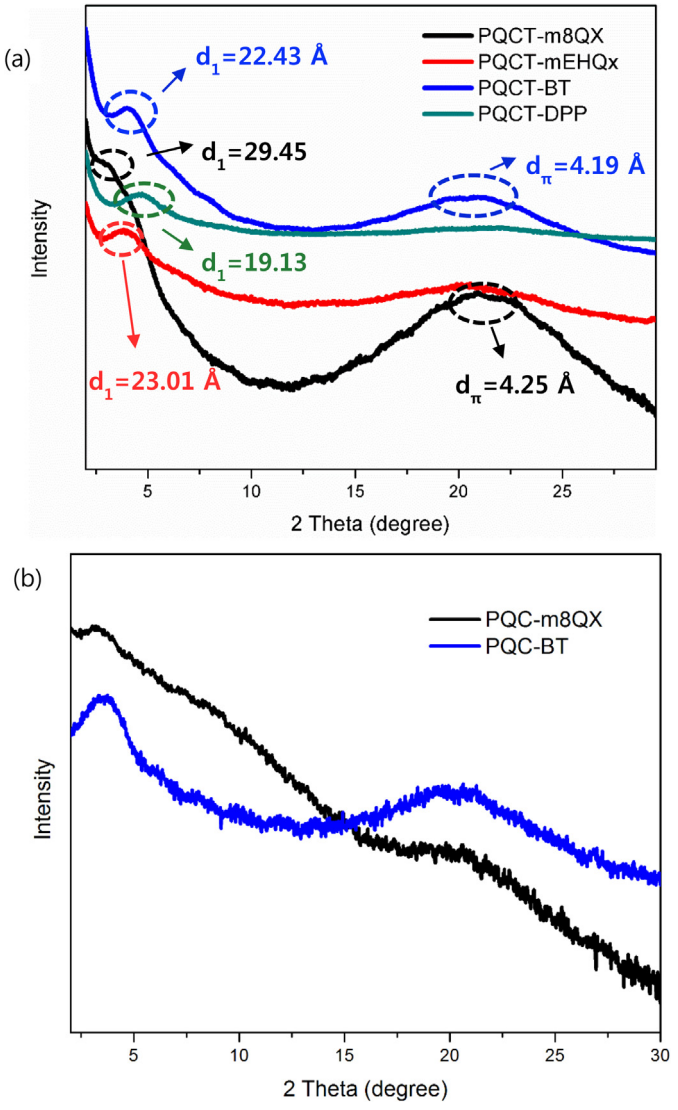

Fig. 5. X-ray diffraction pattern of polymers on a silicon wafer and a polymers (a) out-of-plane and (b) in-plane mode.

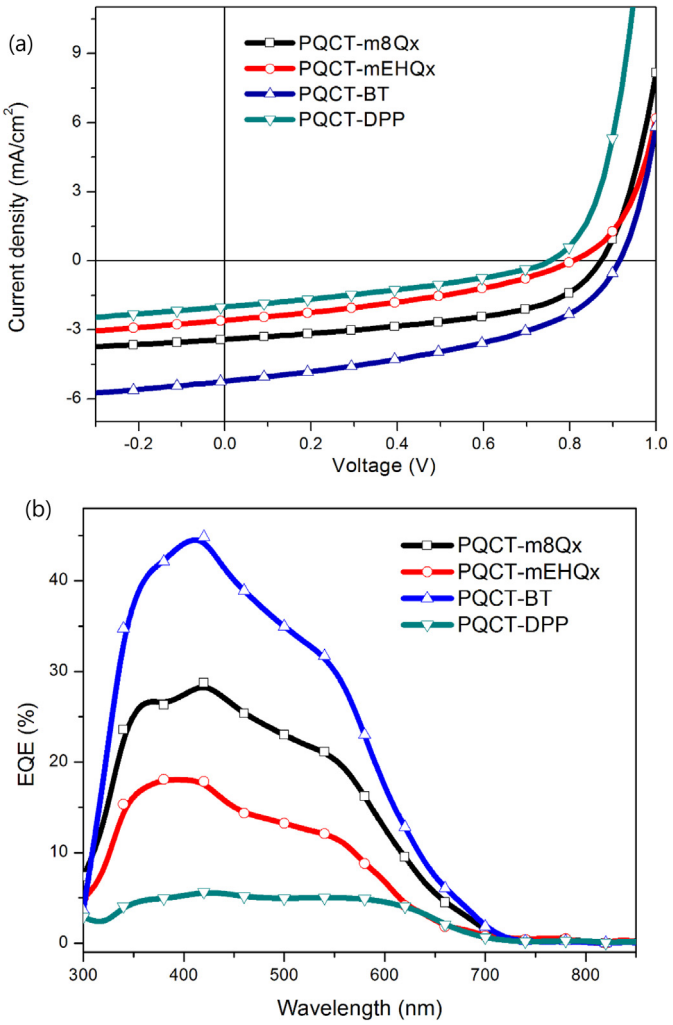

Fig. 6. (a) The J–V curves of the PSC based on polymers:$PC_{70}BM$ under the illumination of AM 1.5G, 100 mW/cm^2, (b) the IPCE spectra of the PSC based on polymers:$PC_{70}BM$.

Additionally, the devices of PQCT-m8Qx, PQCT-mEHQx and PQCT-BT, unlike their UV–vis absorption spectra, wherein the ICT peaks at long wavelength zone were small in shoulder form, they showed EQE values expanded to 750 nm by blending with $PC_{70}BM$. Because PQCT-BT has a high absorption coefficient due to its planar and face-on dominant structure shown in XRD, it possesses the highest J_{SC} of 5.3 mA/cm^2. Additionally, its EQE was highest by 44.8%. PQCT-m8Qx and PQCT-mEHQx generates edge-on riched or weak crystalline structure due to a large dihedral angle inside the molecule, resulting in reduced J_{SC} (3.4 and 2.7 mA/cm^2). The surface morphology of the polymer blend is also a critical factor for determining the efficiency of PSCs.

Therefore, the morphologies of polymer:$PC_{70}BM$ blend films were confirmed by using atomic force microscopy (AFM) and were shown in Fig. 7. The dark-colored and light-colored parts, respectively refer to the $PC_{70}BM$ domains and polymers. The surfaces of PQCT-m8Qx, PQCT-mEHQx and PQCT-BT:$PC_{70}BM$ blended film were smoothed by nanoscale features, while showing low root-mean-square (RMS) roughness of 2.12, 2.36, and 1.97 nm. Additionally, the inter-mixing of polymer and $PC_{70}BM$ was quite easy, so the phase separation of the macro-phase by $PC_{70}BM$ domain was observed. The BHJ structure must have a comparable nanoscale structure to be an effective solar cell since the exciton diffusion length of organic semiconductors is only approximately

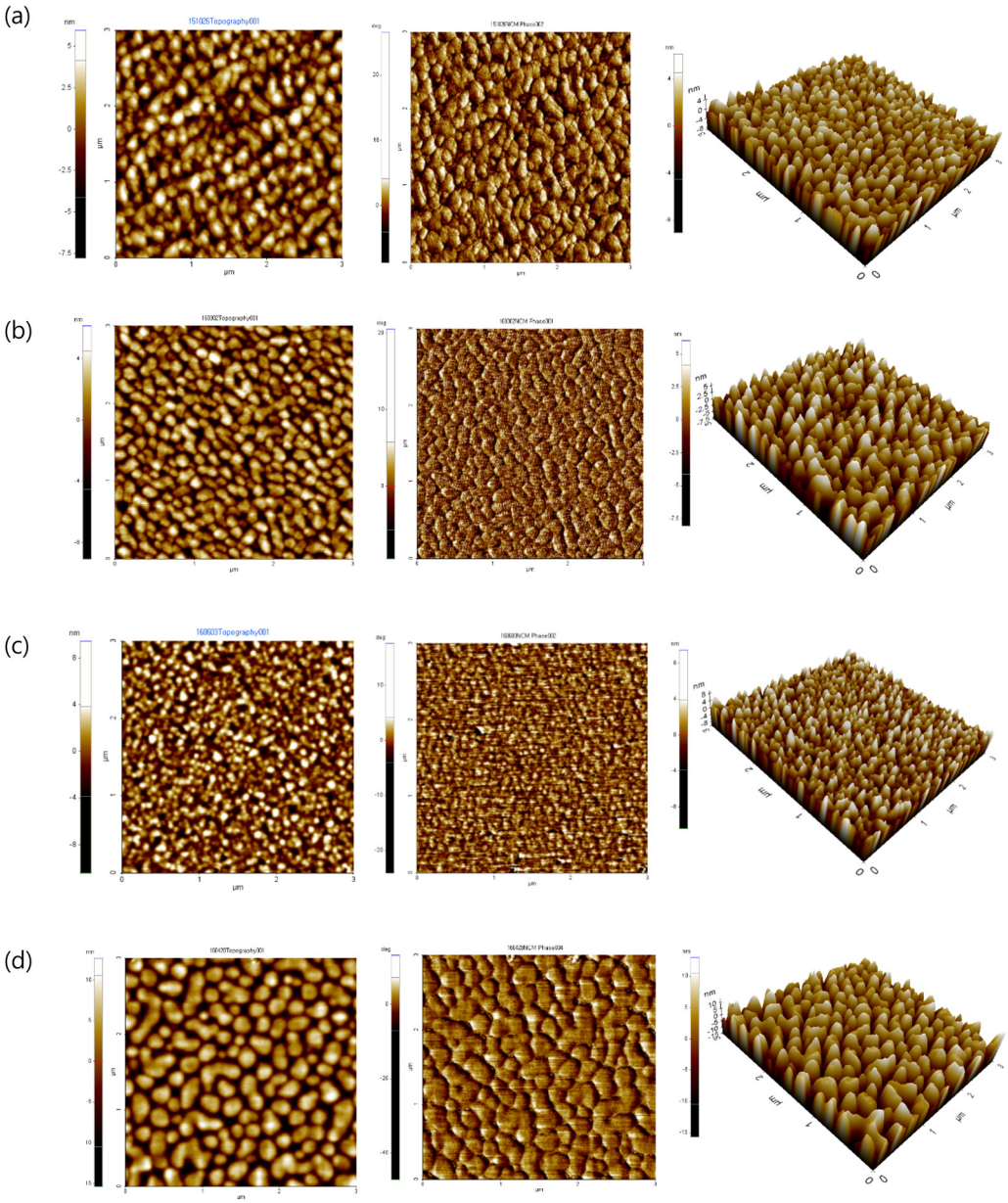

Fig. 7. Topographic AFM images ($3 \times 3\ \mu m^2$) of (a) PQCT-m8Qx:$PC_{70}BM$ = 1:2, (b) PQCT-mEHQx:$PC_{70}BM$ = 1:2, (c) PQCT-BT:$PC_{70}BM$ = 1:2, (d) PQCT-DPP:$PC_{70}BM$ = 1:2.

10 nm [45]. However, PQCT-DPP:$PC_{70}BM$ blended film was measured with high RMS roughness of 4.74 nm, so the exciton separation was not effectively performed. PQCT-DPP showed low J_{SC} (1.9 mA/cm^2), which agrees with the result of the lowest EQE value.

We determined the hole mobility of the polymer and $PC_{70}BM$ blend films from the log J versus log V graphs presented in the Supporting Information, Figs. S4 via a space charge limited current (SCLC) method. A structure of hole-only devices in this work is ITO/PEDOT:PSS/polymer:$PC_{70}BM$/MoO_3/Al. Based on the equation and the log J vs log V graph, the hole mobility values of PQCT-m8Qx, PQCT- mEHQx, PQCT-BT, and PQCT-DPP blended with $PC_{70}BM$ were as follows: $5.74 \times 10^{-4}\ cm^2\ V^{-1}\ s^{-1}$, $4.12 \times 10^{-3}\ cm^2\ V^{-1}\ s^{-1}$, $7.48 \times 10^{-4}\ cm^2\ V^{-1}\ s^{-1}$, and $3.91 \times 10^{-4}\ cm^2\ V^{-1}\ s^{-1}$ respectively. The hole mobility of the polymers was greatly affected by the crystal structure of the polymer film, which influences the charge-transfer pathway. PQCT-BT showed face-on enriched crystallites and PQCT-BT:$PC_{70}BM$ blended film was smoothed by nanoscale features. So, PQCT-BT had the highest hole mobility which led to a high J_{SC} in the fabricated photovoltaic cell. However, PQCT-DPP showed low hole mobility due to the bad exciton separation caused by high RMS roughness.

Conclusions

In this study, by using quinacridone as a donor and different conjugated 2D-side groups as acceptors, four types of polymers were successfully synthesized through a Suzuki coupling reaction. Depending on the chemical structure difference of the side groups that are used as acceptors, the localization behaviors of the electron in the electron distribution of the HOMO through the DFT were shown differently. In comparison with the linear polymer which used the same backbone, the two-dimensional (2D) conjugated side chain polymer exhibits the delocalization of its electron clouds due to the extension of the side chain, resulting in low HOMO level and high V_{OC}. The low dihedral angle of PQCT-BT and the side view were referred to, confirming excellent planarity with a linear structure. Additionally, the XRD results showed the

formation of face-on structure. In the AFM images, polymers except PQCT-DPP showed effective exciton separation in the nano-scale phase and excellent J_{SC} values. When PSC devices with an inverted structure by PQCT-BT:$PC_{70}BM$ (1:2, w/w) were manufactured, V_{OC}, J_{SC} and FF were, respectively, 0.92 V, 5.3 mA/cm^2, and 44.8%, thus achieving the best performance with PCE = 2.2%.

Experimental

Materials

All starting materials were purchased from Sigma Aldrich, Acros, Alfar Aesar or TCI companies and used without further purification. Toluene and tetrahydrofuran (THF) were distilled from benzophenone ketyl and sodium. The following compoundswere synthesized following modified literature procedures 2,9-diboronicester-*N*,*N*′-di(2-octyl-dodecyl)quinacridone (M1) [23], 5-(5-(2-(2,5-dibromothiophen-3-yl)vinyl)thiophen-2-yl)-2,3-bis (3-(octyloxy)phenyl)-8-(thiophen-2-yl)quinoxaline(M2) [16], 5-(5-(2-(2,5-dibromothiophen-3-yl)vinyl)thiophen-2-yl)-2,3-bis (3-(2-ethylhexyloxy)phenyl)-8-(thiophen-2-yl)quinoxaline (M3) [23], 4-(5-(2-(2,5-dibro-mothiophen-3-yl)vinyl)thiophen-2-yl)-5,6-bis(oc-tyloxy)-7-(thiophen-2-yl)benzothiadiazole (M4) [24], (5-(2-(2,5-dibromothiophen-3-yl)vinyl)thi-phen-2-yl)-2,5-bis(2-ethylhexyl)-6-(thiophen-2-yl)pyrrolopyrrole-1,4-dione (M5) [25].

Poly[quinacridone-alt-dithienylvinyl-2,3-bis(3-octyloxy)quinoxaline] (PQCT-m8Qx)

5-(5-(2-(2,5-Dibromothiophen-3-yl)vinyl)thiophen-2-yl)-2,3-bis(3-(octyloxy)phenyl)-8-(thiophen-2-ylquinoxaline (M2) (0.203 g, 0.21 mmol), 2,9-diboronicester-*N*,*N*′-di(2-octyl-dodecyl) quinacridone (M1) (0.236 g, 0.21 mmol), $Pd(PPh_3)_4(0)$ (0.007 g, 0.0063 mmol) and Aliquat 336 were placed in a Schlenk tube, purged with three nitrogen/vacuum cycles, and under a nitrogen atmosphere added 2 M degassed aqueous K_2CO_3 (10 ml) and dry toluene (20 ml). The mixture was heated to 90 °C and stirred for 24 h. After the polymerization was over, the polymer was end-capped with 2-bromothiophene. After reaction quenching, the whole mixture was poured into methanol. The precipitate was filtered off and purified by Soxhlet extraction with solvents in the order methanol, acetone and chloroform. The polymer was recovered from the chloroform fraction and precipitated into methanol. The final product was obtained as a dark red solid after drying in vacuum (0.3 g, 85%). Anal. calcd. For: $C_{112}H_{150}N_4O_4S_3$: C, 78.6; H, 8.8; N, 3.3; O, 3.7; S, 5.6. Found: C, 78.98; H, 8.84; N, 3.64; O, 4.12; S, 4.11%.

Poly[quinacridone-alt-dithienylvinyl-2,3-bis(3-ethylhexyloxy) quinoxaline] (PQCT-mEHQX)

5-(5-(2-(2,5-Dibromothiophen-3-yl)vinyl)thiophen-2-yl)-2,3-bis(3-(2-ethylhexyloxy)phenyl)-8-(thiophen-2-yl)quinoxaline (M3) (0.193 g, 0.20 mmol), 2,9-diboronicester-*N*,*N*′-di(2-octyl-dodecyl)quinacridone (M1) (0.225 g, 0.20 mmol), $Pd(PPh_3)_4(0)$ (0.007 g, 0.006 mmol) and Aliquat 336 were placed in a Schlenk tube, purged with three nitrogen/vacuum cycles, and under a nitrogen atmosphere added 2 M degassed aqueous K_2CO_3 (10 ml) and dry toluene (20 ml). The mixture was heated to 90 °C and stirred for 24 h. After the polymerization was over, the polymer was end-capped with bromothiophene. After reaction quenching, the whole mixture was poured into methanol. The precipitate was filtered off and purified by Soxhlet extraction with solvents in the order methanol, acetone and chloroform. The polymer was recovered from the chloroform fraction and precipitated into methanol. The final product was obtained as a dark violet solid after drying in vacuum (0.29 g, 86%). Anal. calcd. For: $C_{112}H_{150}N_4O_4S_3$: C, 78.6; H, 8.8; N, 3.3; O, 3.7; S, 5.6. Found: C, 76.98; H, 8.36; N, 3.32; O, 4.81; S, 5.83%.

Poly[quinacridone-alt-dithienylvinyl-5,5-bis(octyloxyl) benzothiadiazole] (PQCT-BT)

4-(5-(2-(2,5-Dibro-mothiophen-3-yl)vinyl)thiophen-2-yl)-5,6-bis(oc-tyloxy)-7-(thiophen-2-yl)benzothiadiazole (M4) (0.164 g, 0.20 mmol), 2,9-diboronicester-*N*,*N*′-di(2-octyl-dodecyl)quinacridone (M1) (0.225 g, 0.20 mmol), $Pd(PPh_3)_4(0)$ (0.007 g, 0.006 mmol) and Aliquat 336 were placed in a Schlenk tube, purged with three nitrogen/vacuum cycles, and under a nitrogen atmosphere added 2 M degassed aqueous K_2CO_3 (10 ml) and dry toluene (20 ml). The mixture was heated to 90 °C and stirred in the dark for 24 h. After the polymerization was over, the polymer was end-capped with bromothiophene. After reaction quenching, the whole mixture was poured into methanol. The precipitate was filtered off and purified by Soxhlet extraction with solvents in the order methanol, acetone and chloroform. The polymer was recovered from the chloroform fraction and precipitated into methanol. The final product was obtained as a dark violet solid after drying in vacuum (0.25 g, 81%). Anal. calcd. For: $C_{104}H_{140}N_4O_4S_3$: C, 75.1; H, 9.0,; N, 3.6; O, 4.1; S, 8.2. Found: C, 73.97; H, 8.38; N, 3.52; O, 5.41; S, 7.78%.

Poly[quinacridone-alt-dithienylvinyl-2,5-bis(2-ethylhexyl) diketopyrrolopyrrole] (PQCT-DPP)

(5-(2-(2,5-Dibromothiophen-3-yl)vinyl)thiopen-2-yl)-2,5-bis (2-ethylhexyl)-6-(thiophen-2-yl)pyrrolopyrrole-1,4-dione (M5) (0.158 g, 0.20 mmol), 2,9-diboronicester-*N*,*N*′-di(2-octyl-dodecyl) quinacridone (M1) (0.225 g, 0.20 mmol), $Pd(PPh_3)_4(0)$ (0.007 g, 0.006 mmol) and Aliquat 336 were placed in a Schlenk tube, purged with three nitrogen/vacuum cycles, and under a nitrogen atmosphere added 2 M degassed aqueous K_2CO_3 (10 ml) and dry toluene (20 ml) and DMF (2 ml). The mixture was heated to 90 °C and stirred for 24 h. After the polymerization was over, the polymer was end-capped with bromothiophene. After reaction quenching, the whole mixture was poured into methanol. The precipitate was filtered off and purified by Soxhlet extraction with solvents in the order methanol, acetone and chloroform. The polymer was recovered from the chloroform fraction and precipitated into methanol. The final product was obtained as a dark violet solid after drying in vacuum (0.25 g, 83%). Anal. calcd. For: $C_{98}H_{140}N_4O_4S_3$: C, 76.7; H, 9.2; N, 3.6; O, 4.2; S, 6.3. Found: C, 75.28; H, 8.89; N, 3.57; O, 4.93; S, 6.27%.

Measurements

The ^{1}H NMR (400 MHz) spectra were recorded using a Brüker AMX400 spectrometer in $CDCl_3$, and the chemical shifts were recorded in units of ppm with TMS as the internal standard. The absorption spectra were recorded using an Agilent 8453 UV–vis spectroscopy system. The solutions that were used for the UV–vis spectroscopy measurements were dissolved in chloroform at a concentration of 10 μg/ml. The films were drop-coated from the chloroform solution onto a quartz substrate. All of the GPC analyses were carried out using $CHCl_3$ as the eluent and a polystyrene standard as the reference. The TGA measurements were performed using a TG 209 F3 thermogravimetric analyzer. The cyclic voltammetric waves were produced using a Zahner IM6eX electrochemical workstation with a 0.1 M acetonitrile (substituted with nitrogen for 20 min) solution containing tetrabutylammonium hexafluorophosphate (Bu_4NPF_6) as the electrolyte at a constant scan rate of 50 mV/s. ITO, a Pt wire, and silver/silver chloride [Ag in 0.1 M KCl] were used as the working, counter, and reference electrodes, respectively. The electrochemical potential was calibrated against Fc/Fc+. The HOMO levels of the polymers

were determined using the oxidation onset value. Onset potentials are values obtained from the intersection of the two tangents drawn at the rising current and the baseline changing current of the CV curves. The LUMO levels were calculated from the differences between the HOMO energy levels and the optical band-gaps, which were determined using the UV–vis absorption onset values in the films. The current density–voltage (J–V) curves of the photovoltaic devices were measured using a computer-controlled Keithley 2400 source measurement unit (SMU) that was equipped with a Class A Oriel solar simulator under an illumination of AM 1.5 G (100 mW/cm^2). Topographic images of the active layers were obtained through atomic force microscopy (AFM) in tapping mode under ambient conditions using an XE-100 instrument.

Photovoltaic cell fabrication

All the bulk-heterojunction PV cells were prepared using the following device fabrication procedure. The glass/indium tin oxide (ITO) substrates [Sanyo, Japan (10 Ω/γ)] were sequentially patterned lithographically, cleaned with detergent, ultrasonicated in deionized water, acetone, and isopropyl alcohol, dried on a hot plate at 120 °C for 10 min, and treated with oxygen plasma for 10 min to improve the contact angle just before film coating. Zinc oxide (ZnO) was passed through a 0.45-mm filter before being deposited on ITO at a thickness of ca. 32 nm by spin-coating at 4000 rpm in air, and then dried at 120 °C for 20 min inside a glove box. A blend of 1-(3-methoxycarbonyl)propyl-1-phenyl-[6,6]-C71 ($PC_{70}BM$) and the polymers [1:1–1:4 (w/w)] in *o*-dichlorobenzene was stirred overnight, filtered through a 0.2-μm poly(tetrafluoroethylene) (PTFE) filter, and then spin-coated (500–3000 rpm, 30 s) on top of the ZnO layer. Finally, MoO_3 (5 nm) and Ag anodes (100 nm) were sequentially deposited by thermal evaporation in a high-vacuum chamber (10^{-7} torr). The active area of the fabricated inverted PSC was 7 mm^2.

Hole-only device fabrication and measurement

The hole-only devices were prepared with a diode configuration of ITO(170 nm)/PEDOT:PSS(40 nm)/polymer:$PC_{70}BM$/MoO_3(5 nm)/Al(100 nm). The hole mobility of the active layers was calculated from the SCLC using the J–V curves of the hole-only devices in the dark as follows:

$$J = \frac{9}{8}\varepsilon\varepsilon_0\mu_{h\ (\theta)}\frac{V^2}{L^3}\exp\left(0.89\gamma\sqrt{\frac{V}{L}}\right)$$

where ε_0 is the permittivity of free space (8.85×10^{-14} F/cm); ε is the dielectric constant (assumed to be 3, which is a typical value for conjugated polymers) of the polymer; m is the zero-field mobility of holes (electrons); L is the film thickness; and $V = V_{appl} - V_r - V_{bi}$, where V_{appl} is the applied voltage to the device, V_r is the voltage drop due to series resistance across the electrodes, and V_{bi} is the built-in voltage.

Conflict of interest

The authors declare no competing financial interest.

Acknowledgments

This paper was written as part of Konkuk University's research support program in 2013.

Appendix A. Supplementary data

^{1}H NMR spectrum of polymers, TGA data of polymers, UV-vis absorption spectra and molar absorption coefficients (ε), J–V characteristics of the hole-only devices based on polymer: $PC_{70}BM$ blends. Supplementary data associated with this article can be found, in the online version, at http://dx.doi.org/10.1016/j.jiec.2016.10.044.

References

[1] H.-Y.Y. Chen, J.H. Hou, S.Q. Zhang, Y.Y. Liang, G.W. Yang, Y. Yang, L.P. Yu, Y. Wu, G. Li, Nat. Photonics 3 (11) (2009) 649.
[2] M.H. Choi, K.W. Song, S.W. Heo, Y.W. Han, D.K. Moon, J. Ind. Eng. Chem. 26 (2014) 173.
[3] Z. He, C. Zhong, X. Huang, W.Y. Wong, H. Wu, L. Chen, S. Su, Y. Cao, Adv. Mater. 23 (40) (2011) 4636.
[4] H. Zhou, L. Yang, W. You, Macromolecules 45 (2012) 607.
[5] H.Y. Kim, M.H. Choi, Y.W. Han, D.K. Moon, J.R. Haw, J. Ind. Eng. Chem. 33 (2016) 209.
[6] Q. Fan, Y. Liu, M. Xiao, W. Su, H. Gao, J. Chen, H. Tan, Y. Wang, R. Yang, W. Zhu, J. Mater. Chem. C 3 (2015) 6240.
[7] K. Li, Z. Li, K. Feng, X. Xu, L. Wang, Q. Peng, J. Am. Chem. Soc. 135 (36) (2013) 13549.
[8] L. Huo, T. Liu, B. Fan, Z. Zhao, X. Sun, D. Wei, M. Yu, Y. Liu, Y. Sun, Adv. Mater. 27 (43) (2015) 6969.
[9] S.C. Price, A.C. Stuart, L. Yang, H. Zhou, W. You, J. Am. Chem. Soc. 133 (12) (2011) 4625.
[10] M.C. Scharber, D. Mühlbacher, M. Koppe, P. Denk, C. Waldauf, A.J. Heeger, C.J. Brabec, Adv. Mater. 18 (6) (2006) 789.
[11] B. Yang, Y. Yuan, P. Sharma, S. Poddar, R. Korlacki, S. Ducharme, A. Gruverman, R. Saraf, J. Huang, Adv. Mater. 24 (11) (2012) 1455.
[12] Y.J. Kim, H.N. Kim, M.C. Hwang, Y.H. Kim, C.E. Park, Synth. Met. 198 (2014) 93.
[13] H. Zhou, L. Yang, S. Stoneking, W. You, ACS Appl. Mater. Interfaces 2 (5) (2010) 1377.
[14] J. Ren, X. Bao, L. Han, J. Wang, M. Qiu, Q. Zhu, T. Hu, R. Sheng, M. Sun, R. Yang, Polym. Chem. 6 (2015) 4415.
[15] S. Zhang, Z. Zhang, Y. Li, Adv. Polym. Technol. 32 (2013) (2012) 822.
[16] Z. Gu, P. Tang, B. Zhao, H. Luo, X. Guo, H. Chen, G. Yu, X. Liu, P. Shen, S. Tan, Macromolecules 45 (2012) 2359.
[17] Y. Huang, L. Ye, F. Wu, S. Mei, H. Chen, S. Tan, J. Polym. Sci. A Polym. Chem. 54 (5) (2016) 668.
[18] X. Liu, Y. Huang, Z. Cao, C. Weng, H. Chen, S. Tan, Polym. Chem. 4 (2013) 4737.
[19] J. Chen, M. Xiao, W. Su, X. Duan, L. Duan, W. Peng, H. Tan, R. Yang, W. Zhu, Polymer (United Kingdom) 55 (19) (2014) 4857.
[20] P. Shen, H. Bin, L. Xiao, Y. Li, Macromolecules 46 (24) (2013) 9575.
[21] X. Xu, K. Feng, K. Li, Q. Peng, J. Mater. Chem. A 3 (46) (2015) 23149.
[22] S. De Feyter, A. Gesquire, F.C. De Schryver, U. Keller, K. Mellen, Chem. Mater. 14 (3) (2002) 989.
[23] I. Osaka, M. Akita, T. Koganezawa, K. Takimiya, Chem. Mater. 24 (6) (2012) 1235.
[24] D.H. Kim, H.J. Song, S.W. Heo, K.W. Song, D.K. Moon, Sol. Energy Mater. Sol. Cells 120 (Part A) (2014) 94.
[25] D.H. Yun, H.S. Yoo, K.H. Seong, J.H. Lim, Y.S. Park, J.W. Woot, Appl. Chem. Eng. 25 (5) (2014) 487.
[26] E.D. Gowacki, H. Coskun, M.A. Blood-Forsythe, U. Monkowius, L. Leonat, M. Grzybowski, D. Gryko, M.S. White, A. Aspuru-Guzik, N.S. Sariciftci, Mater. Appl. 15 (12) (2014) 3521.
[27] H.J. Song, D.H. Kim, E.J. Lee, S.W. Heo, J.Y. Lee, D.K. Moon, Macromolecules 45 (19) (2012) 7815.
[28] Z. Gu, P. Shen, S.-W. Tsang, Y. Tao, B. Zhao, P. Tang, Y. Nie, Y. Fang, S. Tan, Chem. Commun. 47 (33) (2011) 9381.
[29] H. Tan, X. Deng, J. Yu, B. Zhao, Y. Wang, Y. Liu, W. Zhu, H. Wu, Yong Cao, Macromolecules 46 (2013) 113.
[30] C.Y. Kuo, Y.C. Huang, C.Y. Hsiow, Y.W. Yang, C.I. Huang, S.P. Rwei, H.L. Wang, L. Wang, Macromolecules 46 (15) (2013) 5985.
[31] T. Wang, A.J. Pearson, D.G. Lidzey, J. Mater. Chem. C (2013) 7266 .
[32] H. Li, C. Gu, L. Jiang, L. Wei, W. Hu, H. Fu, J. Mater. Chem. C 1 (10) (2013) 2021.
[33] L.Y. Liao, W. Zhang, Z. Xiao, J.M. Cao, Z.P. Liu, Q.Q. Zuo, L.M. Ding, Polym. J. 45 (5) (2013) 571.
[34] W. Yue, R.S. Ashraf, C.B. Nielsen, E. Collado-Fregoso, M.R. Niazi, S.A. Yousaf, M. Kirkus, H.Y. Chen, A. Amassian, J.R. Durrant, I. McCulloch, Adv. Mater. 27 (32) (2015) 4702.
[35] X. Zhang, L. Chen, G. Wang, Z.G. Zhang, Y. Li, P. Shen, Synth. Met. 211 (2016) 121.
[36] Y. Wang, Q.F. Yu, H.J. Park, S.H. Ryu, J.H. Choi, U.C. Yoon, Bull. Korean Chem. Soc. 32 (8) (2011) 3081.
[37] M.L. Petrus, R.K.M. Bouwer, U. Lafont, S. Athanasopoulos, N.C. Greenham, T.J. Dingemans, J. Mater. Chem. A 2 (25) (2014) 9474.
[38] C. Duan, R.E.M. Willems, J.J. van Franeker, B.J. Bruijnaers, M.M. Wienk, R.A.J. Janssen, J. Mater. Chem. A 4 (5) (2016) 1855.
[39] D.H. Kim, H.J. Song, E.J. Lee, E.J. Ko, D.K. Moon, Synth. Met. 210 (2015) 304.

[40] K.W. Song, H.J. Song, T.H. Lee, S.W. Heo, D.K. Moon, Polym. Chem. 4 (2013) 3225.
[41] J.J.A. Chen, T.L. Chen, B. Kim, D.A. Poulsen, J.L. Mynar, J.M.J. Fre'chet, B. Ma, ACS Appl. Mater. Interfaces 2 (9) (2010) 2679.
[42] K.H. Hwang, D.H. Kim, M.H. Choi, J.P. Han, D.K. Moon, J. Ind. Eng. Chem. 34 (2016) 66.
[43] M.-H. Choi, E.J. Ko, Y.W. Han, E.J. Lee, D.K. Moon, Polymer 74 (2015) 205.
[44] T. Xu, L. Yu, Mater. Today 17 (1) (2014) 11.
[45] K. Shibasaki, T. Yasuda, Y. Yamamoto, M. Kijima, Polym. Chem. 6 (32) (2015) 5921.